Journal of Physics B: Atomic, Molecular and Optical Physics

Reconstruction of attosecond pulses in the presence of interfering dressing fields using a 100 kHz laser system at ELI-ALPS

OPEN ACCESS
IOP Publishing
Letters
Journal of Physics B: Atomic, Molecular and Optical Physics
J. Phys. B: At. Mol. Opt. Phys. **52** (2019) 23LT01 (7pp)
https://doi.org/10.1088/1361-6455/ab486c

Letter

Reconstruction of attosecond pulses in the presence of interfering dressing fields using a 100 kHz laser system at ELI-ALPS

D Hammerland[1,3], P Zhang[1,3], S Kühn[2], P Jojart[2], I Seres[2], V Zuba[2], Z Varallyay[2], D Charalambidis[2], K Osvay[2], T T Luu[1] and H J Wörner[1]

[1] Laboratorium für Physikalische Chemie, ETH Zürich, Vladamir Prelog-Weg 2, Zürich 8093, Switzerland
[2] ELI-ALPS, ELI-HU Non-Profit Ltd., Dugonics ter 13, Szeged 6720, Hungary

E-mail: trung.luu@phys.chem.ethz.ch

Received 17 June 2019, revised 2 September 2019
Accepted for publication 26 September 2019
Published 7 November 2019

Abstract

Attosecond Pulse Trains (APT) generated by high-harmonic generation (HHG) of high-intensity near-infrared (IR) laser pulses have proven valuable for studying the electronic dynamics of atomic and molecular species. However, the high intensities required for high-photon-energy, high-flux HHG usually limit the class of adequate laser systems to repetition rates below 10 kHz. Here, APT's generated from the 100 kHz, 160 W, 40 fs laser system (HR-1) currently under commissioning at the extreme light infrastructure attosecond light pulse source (ELI-ALPS) are reconstructed using the reconstruction of attosecond beating by interference of two-photon Transitions (RABBIT) technique. These experiments constitute the first attosecond time-resolved photoelectron spectroscopy measurements with attosecond pulses performed at 100 kHz repetition rate and one of the first experiments performed at ELI-ALPS in the framework of projects commissioning its newly installed technologies. These RABBIT measurements were taken with an additional IR field temporally locked to the extreme-ultraviolet APT, resulting in an atypical ω beating. We show that the phase of the 2ω beating recorded under these conditions is strictly identical to that observed in standard RABBIT measurements within second-order perturbation theory. This work highlights an experimental simplification for future experiments based on attosecond interferometry (or RABBIT), which is particularly useful when lasers with high average powers are used.

Keywords: high-harmonic generation, attosecond science, ELI-ALPS, RABBIT

(Some figures may appear in colour only in the online journal)

1. Introduction

Ever since the discovery of high-harmonic generation (HHG) [1], it has proven a valuable source of tabletop vacuum-ultraviolet (VUV) and extreme-ultraviolet (XUV) radiation. As an added benefit over synchrotrons and x-ray free-electron lasers, HHG can produce laser pulses with attosecond temporal duration [2, 3], making it a powerful tool for studying electronic dynamics on sub-femtosecond time scales [4–25]. If a many-cycle infrared (IR) pulse is used for HHG, a set of discrete XUV harmonics are produced, resulting in an attosecond pulse train (APT) [2, 3].

Characterizing these APT's is challenging as traditional methods of measuring spectral phase, such as frequency resolved optical gating (FROG) [26] and spectral phase interferometry for direct electric-field reconstruction [27],

[3] Equally contributed.

usually require passing the pulse through an optical medium, all of which are highly absorptive in the XUV range and thus unsuitable for APT characterization. Variants have been proposed, such as Two-Photon Ionization FROG (TPI-FROG) have been shown as a capable method for VUV pulse characterization [28, 29], but this method is limited to energies around 18 eV, before the Rydberg states of helium lead to resonant contributions to the measured photoelectron signal. VUV and XUV autocorrelators have also been demonstrated [30, 31], but signal stability prevented the FROG algorithm from being effectively applied. As a result, the reconstruction of attosecond beating by interference of two-photon transitions (RABBIT) is frequently used for the characterization of APT's [3, 32, 33]. In this method, two adjacent harmonics photoionize an atom in the presence of a long-wavelength field, usually the generating IR field, resulting in the creation of side bands in the photoelectron spectra between the characteristic harmonics. The corresponding side-band intensity beats at twice the angular frequency of the IR pulse with an offset phase corresponding to the spectral-phase difference of the neighboring harmonics and the atomic phases [34]. These atomic phases have been measured experimentally and can be reasonably predicted by theory for atoms [10] and molecules [35], allowing for the isolation of the XUV spectral phase, which enables the reconstruction of the APT.

A critical aspect of progressing the application of APT's is increasing the repetition rates of the generating IR laser systems. Historically, the peak intensities necessary for high-flux or high-photon-energy HHG, typically $>10^{14}$ W cm^{-2}, have meant that viable laser systems were limited to amplifiers bottle-necked to less than 10 kHz repetition rates. Although other methods such as enhancement cavities [36–38] or tight-focusing geometries with lower pulse power [39–42] have achieved HHG at higher repetition rates, both methods introduce additional experimental challenges that can limit their applicability. The extreme light infrastructure attosecond light pulse source (ELI-ALPS) facility [43] has been designed in order to push the frontiers of attosecond science. This facility boasts the High Repetition-1 (HR-1) laser system that is currently under commissioning as part of a R&D consortium with Active Fiber Systems GmbH. The system is planned to eventually produce >1 mJ pulses with sub-7 fs pulses at 100 kHz, making it the first of a new generation of high-pulse-energy, high-repetition-rate, femtosecond laser systems.

A considerable challenge of applying these high-average-power systems is the thermal load on the optical components, resulting from even small fractions of the absorbed high average laser power. This is particularly problematic for the sub-micron metallic foils that are frequently used to filter the XUV light from its generating IR light. We developed a theoretical extension of RABBIT that incorporates residual generating IR light that is temporally locked to the XUV APT to model experiments performed without metallic filters. The main effect of this additional field is the appearance of

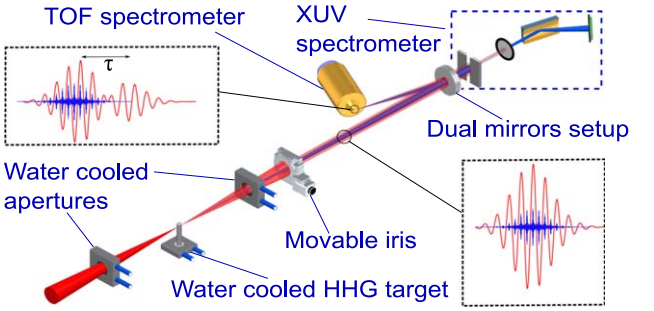

Figure 1. Schematic of the attosecond beamline. TOF: time-of-flight electron spectrometer.

side-band oscillations at ω, the angular frequency of the IR, in addition to the traditional 2ω oscillation. Previous RABBIT measurements have shown ω oscillations [44,45], however, these arose from the interference of the dressing IR light that was present during the HHG process as a consequence of the experimental geometry, which led to an ω modulation of the high-harmonic flux. The ω oscillations reported in our work in contrast arise from a linear interference of the IR dressing field with a constant XUV flux, as illustrated in figure 1. In this work, we show that inspite of the presence of the ω oscillations, the 2ω oscillations still encode the same information as traditional RABBIT measurements performed in the absence of the locked IR field. This method proves to be a valuable extension of the traditional measurement schemes as it captures the same information as traditional RABBIT, but operates without the need for eliminating the IR field residual from the HHG process, e.g. with the help of fragile metallic filters.

Section 2 of this work describes the HR-1 laser system, the beamline used for our experiments, and further discusses the challenges of working with high-repetition-rate, high-pulse-energy laser systems. Section 3 focuses on the effect of the temporally locked IR pulse on the RABBIT experiments. Section 4 details a method of reconstruction of the XUV APT and applies it to the XUV field used in this work. Section 5 summarizes the results.

2. Experimental setup

2.1. The HR-1 laser system

The APT was generated using the state-of-the-art HR-1 laser system [43]. The ytterbium-fiber, chirped-pulse amplifier consists of eight separate amplifiers that are temporally synchronized to output 3 mJ, 200 fs, laser pulses of central wavelength 1030 nm at 100 kHz, summing to 300 W average power. After the main amplifier, the beam passes through a hollow-core-fiber compression stage where self-phase-modulation broadens the spectrum to support a 40 fs pulse. The 1.6 mJ pulses exiting the fiber are actively pointing stabilized with a beam-pointing system and then diverted through a half-wave-plate and a thin-film polarizer to implement a continuous power adjustment. The high average power of the

laser system inhibited the use of even dedicated high power irises for beam diameter adjustment. As a result, the beam is expanded using ultraviolet-grade fused silica lenses and a water-cooled 20 mm aperture (fixed diameter iris) to a $1/e^2$ diameter of 15 mm. In this configuration, the maximally available average power is around 120 W. Prior to entering the attosecond end station, the pulse duration is compressed to ~40 fs using a chirped-mirror compressor.

2.2. HHG and attosecond beamline

The attosecond beamline used with the HR-1 laser is shown in figure 1. The beamline was transported to and installed at ELI-ALPS for a series of collaborative experimental campaigns of the ETH team. The laser light was focused for HHG using a 350 mm focal length, 1030 nm high-reflectivity, spherical mirror. The HHG target was a custom-made finite gas-cell chamber with a stainless steel target encapsulated in a differentially pumped cell (excluded for clarity). The metal target was backed with 300–400 mbar of argon.

After HHG, the emitted harmonics and co-propagating IR fields passed concentrically through an 8 mm hard aperture for heat dissipation. This attenuates the IR sufficiently that a motorized iris can be positioned such that its opening is concentric with the XUV light. The iris opening diameter was then adjusted such that the IR intensity would only induce single-photon transitions during the RABBIT measurements [44]. The co-propagating IR light is helpful in the alignment of the XUV light into an XUV spectrometer. The XUV light is incident at 3° onto a variable-line-spacing grating that then disperses the XUV light onto an imaging multi-channel plate (MCP) that emits onto a phosphor screen for detection with a camera. An anodized aluminum blocker is used to prevent the zeroth-order reflection from damaging the MCP.

After the HHG spectrum has been optimized, a passively stable dual-mirror assembly is inserted into the beam path for focusing the IR and XUV light onto the target. A piezo-controlled stage is used to adjust the time delay, τ, between the XUV and IR pulses. The inner mirror was a custom-made XUV multi-layer mirror (AXO Dresden GmbH) with a reflectivity designed to be centered at ~43 eV with a ~7 eV bandwidth, as shown in figure 2. By dividing the static XUV-only PES from neon by the photoionization cross section, as shown in figure 2, the XUV spectra can be determined. This demonstrates how the mirror allows for the isolation of a small group of XUV harmonics. This XUV mirror has a radius of curvature (ROC) of 0.5 m. The outer mirror was a high-reflectivity, 1030 nm optic, also with a ROC of 0.5 m. The XUV and IR light were then focused in front of a 0.5 m field-free time-of-flight (TOF) spectrometer, which has been described in detail in [45].

After the light passes through the sample, it is guided towards an imaging setup. This allows for fine positioning of the sample target and beam focus relative to the TOF skimmer. Further, it can be used to monitor the IR beam positions and focal parameters.

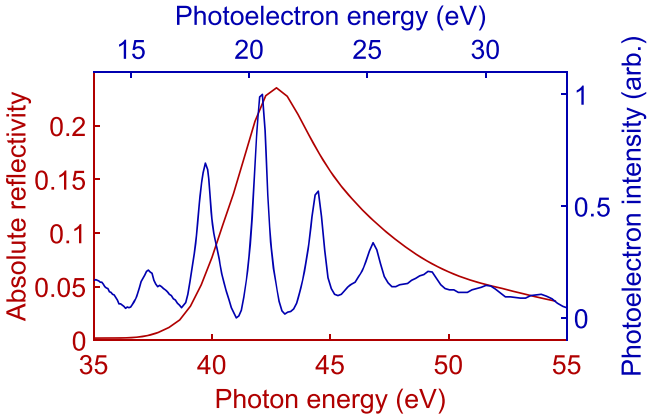

Figure 2. Plot of the absolute XUV mirror reflectivity (red) and the cross-section-corrected XUV-only photoelectron spectrum (blue) (PES). This is obtained by dividing a measured PES by the photoionization cross section at a particular photon energy. The result is the approximate XUV photon spectrum.

2.3. 100 kHz considerations

Two major challenges of using high-intensity, high-repetition-rate laser systems are managing the high thermal load on the optics and the high speed of data acquisition. When working with an average power output exceeding 100 W, even a 99% reflectivity results in enough optical power absorption to cause wavefront distortion from local heating of the optics. As a result, it was critical to use highly reflective, greater than 99.9% reflectivity, 1030 nm optics for all guiding elements and for focusing into the HHG chamber and interaction region of the TOF spectrometer.

An additional problem that arose was the impossibility to use metallic foils for filtering the XUV light from the generating IR light. These 200 nm aluminum foils (Lebow Company) melted at incident-power levels of only 10 W. The theoretical implications of this additional temporally locked IR field on the measured data are addressed in section 4. The inability to filter the IR from the XUV led to high average IR powers being incident on the metallic XUV mirror. This, paired with the relatively lower IR reflectivity of the XUV mirror, resulted in the XUV mirror experiencing notable thermal expansion. However, the imaging setup did not reveal notable thermally induced deformation of the XUV mirror, as seen by the stability of the IR beam profile during operation. Any heat-related temporal distortion of the measurement was prevented by allowing the XUV mirror to thermalize before scans. During the thermalization, the PES generated was constant, suggesting negligible distortion of our XUV pulses.

Wherever beam attenuation was needed considerable efforts were made to dissipate heat actively in order to optimize stability. Custom water-cooled elements were added throughout the system, as shown in figure 1. The 15 mm hard aperture before the chirped mirror compressor and the post-HHG, 8 mm, hard aperture are both connected to a closed, chilled water loop that was used to dissipate approximately 20 W and 35 W, respectively. The HHG target featured a similar cooling system. This increased the stability of the HHG and mitigated thermal damage to the HHG target.

In order to record the time-of-flight signals at high repetition rate, we employed a high-speed digitizer (Keysight Technologies U5309A PCIe, 2 GS/s, 2 channels, 8 bits) directly connected to the MCP output. Although Keysight Technologies could provide the firmware option to do on-the-fly averaging, we found that the triggered simultaneous acquisition and readout mode already supports real-time acquisition at 100 kHz. By making use of the ring buffer, optimal direct memory access transfer can be obtained such that each data transfer is very close to one megabyte per transfer. In this case, a LabVIEW virtual instrument can be written to simultaneously record and transfer the data from the digitizer to the computer in parallel. As a result, we can record the full time-of-flight spectrum for every laser shot using the digitizer and average the signals on the CPU in real time at 100 kHz for time-of-flight intervals of 400 ns. This is sufficient for all of the measurements presented in this work. For longer time-of-flight intervals the actual acquisition speed drops but even for extremely long intervals, the achievable recording speed hardly falls below 50 kHz. By repeating the data acquisition and averaging for every time delay, we obtained the RABBIT traces, making use of all of the laser shots at 100 kHz.

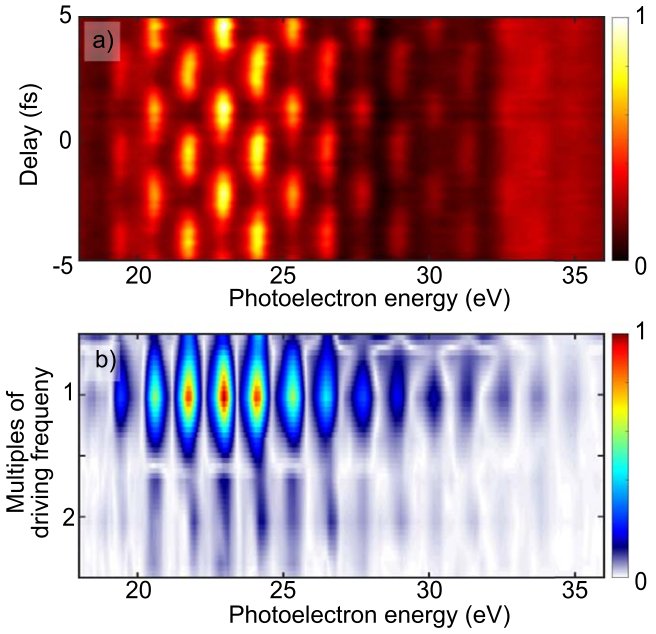

Figure 3. False-color representation of (a) the attosecond PES scan, (b) the Fourier transform amplitude of the scan along the time axis, showing oscillations with angular frequencies of both ω and 2ω.

3. Results

As mentioned in section 2.3, a notable challenge of high-average-power HHG experiments comes when attempting to isolate the XUV photons from their generating IR light. Sub-micron metallic foils have been historically used to remove the IR light and compensate for the attochirp. These foils, however, are notoriously fragile and cannot handle the high average power present in high-repetition-rate, high-pulse-energy laser systems. Annular beams can be used to generate spatially separated XUV and IR pulses. This approach was demonstrated as early as 1994 [46], subsequently used in a number of experiments (e.g. [3, 44, 45]) and recently extended to high-power lasers [47] and few-cycle pulses [48]. The masks used in the early works to block out the central area of the generating beam are not compatible with high-average-power lasers. The drilled mirrors, used in the more recent works, sacrifice a fraction of the laser power that would otherwise be available for the HHG process. Other methods have also been implemented for separating IR and XUV light, such as utilizing the diffraction from a micro-channel plate [49], grating pairs [50], or relying on the frequency dependence in Brewster's angle to transmit IR and reflect XUV [51]. While extremely useful, these methods have not yet been demonstrated at the high average powers used in this work.

In this work, a new method is introduced and demonstrated wherein the IR light was not separated from the XUV light, but rather used in combination with the delayed IR light. This additional laser field can be easily incorporated in the common RABBIT framework by introducing a second IR field that is temporally locked to the XUV APT. Adding this field and following through the standard RABBIT derivations (see appendix), the typical RABBIT sideband oscillations [34]

$$SB(\tau) \propto \cos\left(2\omega\tau + \Delta\phi_{\mathrm{XUV}} + \Delta\phi_{\mathrm{atomic}}\right), \qquad (1)$$

are still preserved, although they are additionally accompanied by oscillations at angular frequency ω. Nevertheless, the phases of the 2ω oscillations are strictly identical to the situation encountered in traditional RABBIT experiments. In equation (1) $\Delta\phi_{\mathrm{XUV}}$ represents the spectral-phase difference between the next-higher and next-lower harmonic orders, whereas $\Delta\phi_{\mathrm{atomic}}$ represents the corresponding atomic-phase difference.

The relative intensity of the ω and 2ω oscillations is proportional to the relative intensity of the delayed and locked IR fields. In the limit of a zero-intensity locked IR field, the standard RABBIT scheme is recovered and the 2ω oscillations dominate. When the delayed IR is of zero intensity, a static spectrum is expected. These limits were observed during the implementation of the experiment.

Figure 3(a) shows an attosecond PES trace measured in neon. The 1030 nm generating field has an optical period of 3.4 fs, which dominates the oscillations. However, Fourier transformation along the temporal-delay axis, shown in figure 3(b), reveals that weaker 2ω oscillations are also present in the data. This places the measurement in the limit of a weak delayed IR field relative to the locked IR field and proves that the measurements were taken in the perturbative limit with respect to the IR fields.

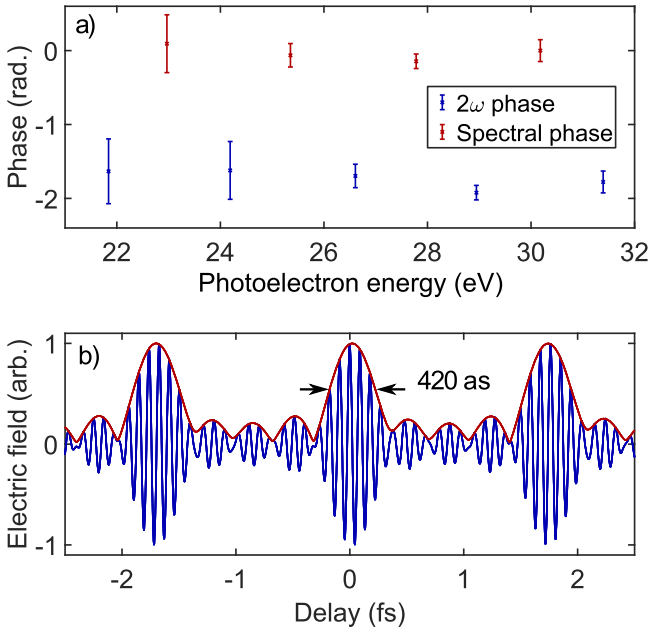

Figure 4. Reconstruction of the APT. (a) Phase extracted from the 2ω oscillations shown in figure 3 and reconstructed spectral phase, after taking into account the atomic phases, (b) attosecond structure of the generated APT (blue) and its envelope (red). τ represents the full width at half maximum (FWHM) of the electric-field envelope of ~420 as, corresponding to an intensity FWHM of ~290 as. The carrier-envelope phase of the APT was chosen randomly for illustration purposes as it was not determined by our present measurements.

4. Pulse reconstruction

The phase of the 2ω oscillation in each sideband was extracted by taking the argument of the complex average of the Fourier transform across the photoelectron-energy bandwidth of each sideband. The phases of the sidebands are plotted (blue) in figure 4(a). The reflective properties of the inner multilayer XUV mirror incorporate a linear-chirp compensation, which removes the quadratic component of the spectral phase, as seen in the reconstructed phases in figure 4(a) (red). From each of these values, the difference of the atomic phases of the neighboring harmonics taken from [10] were subtracted to determine the XUV spectral phase, $\Delta\phi_{\mathrm{XUV}}$, by concatenation. More precisely, the highest-energy sideband was chosen for the zero-phase value in the reconstruction and the relative phases of the harmonics were then found by successively adding the phase difference from one harmonic to the next. We note that the determination of accurate error bars from these measurements represents a significant challenge, as instability in gas pressure, laser fluctuations, mirror assembly temperature and stability all play a significant role but cannot be recorded on a shot-to-shot basis. Here they were approximated by adding in quadrature the scan-normalized signal-to-noise ratios with the standard deviation of the weighted phase values.

The spectral intensity of each harmonic was produced by dividing the PES by the associated neon 2p photoionization cross section [52]. Delta functions at the XUV harmonic energy were assumed to approximate the APT near the center of the pulse. These fields were superimposed with their corresponding relative phases and the intensities in order to reconstruct the APT, figure 4(b) (blue), near the center of the pulse. We note that the carrier envelope phase of the XUV APT cannot be determined within the RABBIT approach and has therefore been chosen randomly.

5. Conclusion and outlook

This paper describes the first attosecond time-resolved experiments realized in the ELI-ALPS facility and marks the first demonstration of 100 kHz attosecond PES, representing a substantial step forward in the development of table-top attosecond experiments. These higher acquisition rates open up exciting avenues for emission-angle-resolved attosecond photoelectron spectroscopy in all phases of matter and will be particularly valuable for electron-ion-coincidence measurements that currently remain repetition-rate limited.

The RABBIT technique has been tailored to work with an additional IR pulse temporally locked to the XUV APT. The manifestation of this pulse in the PES is an ω oscillation in addition to the usual 2ω oscillation. Theoretically, the 2ω oscillations were shown to encode identical information as in the standard RABBIT scheme. This opens the possibility of performing RABBIT measurements without the need for fragile filters and will thereby benefit attosecond pulse metrology as well as measurements of attosecond photoionization delays at high repetition rates and high average powers.

Acknowledgments

The authors acknowledge the contributions of Dr Arohi Jain and Dr Thomas Gaumnitz to the preparatory phase of this work, such as the installation of the attosecond beamline at the ELI-ALPS facility, as well as optical and mechanical adaptations for the operation at high laser repetition rates. The authors especially acknowledge all of the staff at the ELI-ALPS laser facility for their efforts throughout the beam times, particularly Dr Tamás Csizmadia and Dr Miklós Füle, the technical staff of the ETH Zürich Laboratorium für Physikalische Chemie, particularly Andreas Schneider for help with electronics as well as Mario Seiler and Markus Kerellaj for the custom-manufactured mechanical parts used during the experiment and Dr Adam Smith, Danylo Matselyukh, and Jakub Kocák for fruitful discussions and proofreading. This research was funded by ETH Zürich and the Swiss National Science Foundation through grants 200021E_162822 and 200021_172946 as well as the ELI-ALPS project (GINOP-2.3.6-15-2015-00001), which is supported by the European Union and co-financed by the European Regional Development Fund.

Appendix

Here, we derive the expressions for the side-band-intensity oscillations relevant for the interpretation of the present experimental results. For simplicity, we restrict the description of the XUV APT to that of two neighboring harmonics of orders $q+1$ and $q-1$

$$E_{\mathrm{XUV}}(t) = (A_{q+1}e^{i(\phi_{q+1}-(q+1)\omega t)} + A_{q-1}e^{i(\phi_{q-1}-(q-1)\omega t)} + \mathrm{C.C.}), \quad (A.1)$$

where ϕ_{q+1} and ϕ_{q-1} are the relevant spectral-phase components and C.C. stands for complex conjugate. We further describe the IR field as consisting of two components, one that is temporally locked to the XUV APT and one that is delayable (with delay τ) with respect to it:

$$E_{IR}(\tau, t) = (A_{\mathrm{locked}}\, e^{i(\phi_{\mathrm{rel}}-\omega t)} + A_{\mathrm{delayed}}\, e^{i\omega(\tau-t)} + \mathrm{C.C.}). \quad (A.2)$$

Following the standard framework of second-order perturbation theory of RABBIT, the induced polarization of the combined XUV and IR pulses describing two-color two-photon ionization of an atom can be written as

$$\begin{aligned} P(\tau, t) \propto\ & (A_{\mathrm{locked}}\, e^{i(\phi_{\mathrm{rel}}-\omega t)} + A^{*}_{\mathrm{locked}}\, e^{-i(\phi_{\mathrm{rel}}-\omega t)} \\ & + A_{\mathrm{delayed}}\, e^{i\omega(\tau-t)} + A^{*}_{\mathrm{delayed}}\, e^{-i\omega(\tau-t)}) \\ & \times (A_{q+1}e^{i(\phi_{q+1}+\phi^{\mathrm{at}}_{q+1}-(q+1)\omega t)} \\ & + A_{q-1}e^{i(\phi_{q-1}+\phi^{\mathrm{at}}_{q-1}-(q-1)\omega t)} + \mathrm{C.C.}), \end{aligned} \quad (A.3)$$

where ϕ^{at}_{q+1} and ϕ^{at}_{q-1} are the relevant atomic phases resulting from two-color two-photon ionization. Hence, the result is merely the superposition of two RABBIT-like polarizations, one generated from the locked IR field and one generated from the delayed IR field:

$$\begin{aligned} P(\tau, t) \propto\ & A_{\mathrm{delayed}}A_{q+1}e^{i(-(q+2)\omega t-\omega\tau+\phi_{q+1}+\phi^{\mathrm{at}}_{q+1})} \\ & + A^{*}_{\mathrm{delayed}}A_{q+1}e^{i(-q\omega t+\omega\tau+\phi_{q+1}+\phi^{\mathrm{at}}_{q+1})} \\ & + A_{\mathrm{delayed}}A_{q-1}e^{i(-q\omega t-\omega\tau+\phi_{q-1}+\phi^{\mathrm{at}}_{q-1})} \\ & + A^{*}_{\mathrm{delayed}}A_{q-1}e^{i(-(q-2)\omega t+\omega\tau+\phi_{q-1}+\phi^{\mathrm{at}}_{q-1})} \\ & + A_{\mathrm{locked}}A_{q+1}e^{i(-(q+2)\omega t+\phi_{\mathrm{rel}}+\phi_{q+1}+\phi^{\mathrm{at}}_{q+1})} \\ & + A^{*}_{\mathrm{locked}}A_{q+1}e^{i(-q\omega t-\phi_{\mathrm{rel}}+\phi_{q+1}+\phi^{\mathrm{at}}_{q+1})} \\ & + A_{\mathrm{locked}}A_{q-1}e^{i(-q\omega t+\phi_{\mathrm{rel}}+\phi_{q-1}+\phi^{\mathrm{at}}_{q-1})} \\ & + A^{*}_{\mathrm{locked}}A_{q-1}e^{i(-(q-2)\omega t-\phi_{\mathrm{rel}}+\phi_{q-1}+\phi^{\mathrm{at}}_{q-1})} \\ & + \mathrm{C.C.} \end{aligned} \quad (A.4)$$

Examining the polarization at frequency $q\omega$, corresponding to the side-band oscillation we find

$$\begin{aligned} P_q(\tau, t) \propto\ & A^{*}_{\mathrm{delayed}}A_{q+1}e^{i(-q\omega t+\omega\tau+\phi_{q+1}+\phi^{\mathrm{at}}_{q+1})} \\ & + A_{\mathrm{delayed}}A_{q-1}e^{i(-q\omega t-\omega\tau+\phi_{q-1}+\phi^{\mathrm{at}}_{q-1})} \\ & + A^{*}_{\mathrm{locked}}A_{q+1}e^{i(-q\omega t-\phi_{\mathrm{rel}}+\phi_{q+1}+\phi^{\mathrm{at}}_{q+1})} \\ & + A_{\mathrm{locked}}A_{q-1}e^{i(-q\omega t+\phi_{\mathrm{rel}}+\phi_{q-1}+\phi^{\mathrm{at}}_{q-1})}. \end{aligned} \quad (A.5)$$

The intensity oscillation at the relevant 2ω frequency $S_{q,2\omega}(\tau)$ is

$$S_{q,2\omega}(\tau) \propto |F[P_{q,2\omega}(\tau, t)]|^2 \propto 2 + 2\cos(2\omega\tau + \phi_{q+1} - \phi_{q-1} + \phi^{\mathrm{at}}_{q+1} - \phi^{\mathrm{at}}_{q-1}), \quad (A.6)$$

where $F[P(t)]$ is the notation for Fourier transform of $P(t)$, which is identical with the standard RABBIT situation and is reproduced as equation (1) in the main text, with the correspondence $\Delta\phi_{\mathrm{XUV}} = \phi_{q+1} - \phi_{q-1}$ and $\Delta\phi_{\mathrm{atomic}} = \phi^{\mathrm{at}}_{q+1} - \phi^{\mathrm{at}}_{q-1}$.

ORCID iDs

P Zhang https://orcid.org/0000-0001-7746-2113
T T Luu https://orcid.org/0000-0003-3772-3379
H J Wörner https://orcid.org/0000-0002-8877-0872

References

[1] Ferray M 1988 *J. Phys. B: At. Mol. Opt. Phys.* **21** L31 McPherson A, Gibson G, Jara H, Johann U, Luk T S, McIntyre I A, Boyer K and Rhodes C K 1987 *J. Opt. Soc. Am. B* **4** 595–601
[2] Antoine P, L'huillier A and Lewenstein M 1996 *Phys. Rev. Lett.* **77** 1234–7
[3] Paul M P, Toma S E, Breger P, Mullot G, Auge F, Balcou P, Muller G H and Agostini P 2001 *Science* **292** 1689–92
[4] Schultze M *et al* 2010 *Science* **328** 1658–62
[5] Klünder K *et al* 2011 *Phys. Rev. Lett.* **106** 143002
[6] Dahlström J M, L'Huillier A and Maquet A 2012 *J. Phys. B: At. Mol. Opt. Phys.* **45** 183001
[7] Dahlström J M, Carette T and Lindroth E 2012 *Phys. Rev.* A **86** 061402
[8] Guénot D *et al* 2012 *Phys. Rev.* A **85** 053424
[9] Guénot D *et al* 2014 *J. Phys. B: At. Mol. Opt. Phys.* **47** 245602
[10] Palatchi C, Dahlström J M, Kheifets A S, Ivanov I A, Canaday D M, Agostini P and Dimauro L F 2014 *J. Phys. B: At. Mol. Opt. Phys.* **47** 245003
[11] Heuser S *et al* 2016 *Phys. Rev.* A **94** 1–10
[12] Huppert M, Jordan I, Baykusheva D, Von Conta A and Wörner H J 2016 *Phys. Rev. Lett.* **117** 1–6
[13] Jordan I, Huppert M, Pabst S, Kheifets A S, Baykusheva D and Wörner H J 2017 *Phys. Rev.* A **95** 013404
[14] Loriot V *et al* 2017 *J. Opt.* **19** 114003
[15] Bray A W, Naseem F and Kheifets A S 2018 *Phys. Rev.* A **97** 1–12
[16] Vos J, Cattaneo L, Patchkovskii S, Zimmermann T, Cirelli C, Lucchini M, Kheifets A S, Landsman A S and Keller U 2018 *Science* **360** 1326–30
[17] Goldsmith C, Jaroń-Becker A and Becker A 2019 *Appl. Sci.* **9** 492
[18] Takahashi E J, Lan P, Mücke O D, Nabekawa Y and Midorikawa K 2013 *Nat. Commun.* **4** 2691
[19] Okino T, Furukawa Y, Nabekawa Y, Miyabe S, Amani Eilanlou A, Takahashi E J, Yamanouchi K and Midorikawa K 2015 *Sci. Adv.* **1** e1500356
[20] Wang H, Chini M, Chen S, Zhang C H, He F, Cheng Y, Wu Y, Thumm U and Chang Z 2010 *Phys. Rev. Lett.* **105** 143002
[21] Li J *et al* 2017 *Nat. Commun.* **8** 186
[22] Gaumnitz T, Jain A, Pertot Y, Huppert M, Jordan I, Ardana-Lamas F and Wörner H J 2017 *Opt. Express* **25** 27506

[23] Popmintchev T *et al* 2012 *Science* **336** 1287–91
[24] Schultze M *et al* 2014 *Science* **346** 1348–52
[25] Hammond T J, Brown G G, Kim K T, Villeneuve D M and Corkum P B 2016 *Nat. Photon.* **10** 171–5
[26] Trebino R and Kane D J 1993 *J. Opt. Soc. Am.* A **10** 1101–11
[27] Iaconis C and Walmsley I A 1998 *Opt. Lett.* **23** 792–4
[28] Sekikawa T, Katsura T, Miura S and Watanabe S 2002 *Phys. Rev. Lett.* **88** 193902
[29] Sekikawa T, Kanai T and Watanabe S 2003 *Phys. Rev. Lett.* **91** 103902
[30] Tzallas P, Charalambidis D, Papadogiannis N A, Witte K and Tsakiris G D 2005 *J. Mod. Opt.* **52** 321–38
[31] Nabekawa Y, Shimizu T, Okino T, Furusawa K, Hasegawa H, Yamanouchi K and Midorikawa K 2006 *Phys. Rev. Lett.* **97** 153904
[32] Veniard V, Taieb R and Maquet A 1996 *Phys. Rev.* A **54** 721–8
[33] Muller H G 2002 *Appl. Phys.* B **74** 17–21
[34] Dahlström J M, Guénot D, Klünder K, Gisselbrecht M, Mauritsson J, L'Huillier A, Maquet A and Taïeb R 2013 *Chem. Phys.* **414** 53–64
[35] Baykusheva D and Wörner H J 2017 *J. Chem. Phys.* **146** 124306
[36] Jones R J, Moll K D, Thorpe M J and Ye J 2005 *Phys. Rev. Lett.* **94** 1–4
[37] Pupeza I *et al* 2013 *Nat. Photon.* **7** 608–12
[38] Carstens H *et al* 2016 *Optica* **3** 366
[39] Boullet J, Zaouter Y, Limpert J, Petit S, Mairesse Y, Fabre B, Higuet J, Mével E, Constant E and Cormier E 2009 *Opt. Lett.* **34** 1489
[40] Vernaleken A *et al* 2011 *Opt. Lett.* **36** 3428
[41] Rothhardt J, Hädrich S, Klenke A, Demmler S, Hoffmann A, Gotschall T, Eidam T, Krebs M, Limpert J and Tünnermann A 2014 *Opt. Lett.* **39** 5224
[42] Harth A *et al* 2017 *J. Opt.* **20** 014007
[43] Kühn S *et al* 2017 *J. Phys. B: At. Mol. Opt. Phys.* **50** 132002
[44] Swoboda M, Dahlstrom J M, Ruchon T, Johnsson P, Mauritsson J, L'Huillier A and Schafer K J 2009 *Laser Phys.* **19** 1591–9
[45] Jordan I, Jain A, Gaumnitz T, Ma J and Wörner H J 2018 *Rev. Sci. Instrum.* **89** 053103
[46] Peatross J, Chaloupka J L and Meyerhofer D D 1994 *Opt. Lett.* **19** 942
[47] Klas R, Kirsche A, Tschernajew M, Rothhardt J and Limpert J 2018 *Opt. Express* **26** 19318
[48] Gaumnitz T, Jain A and Wörner H J 2018 *Opt. Lett.* **43** 4506
[49] Zhang Q, Zhao K, Li J, Chini M, Cheng Y, Wu Y, Cunningham E and Chang Z 2014 *Opt. Lett.* **39** 3670
[50] Frassetto F, Villoresi P and Poletto L 2008 *J. Opt. Soc. Am.* A **25** 1104
[51] Takahashi E J, Hasegawa H, Nabekawa Y and Midorikawa K 2004 *Opt. Lett.* **29** 507
[52] Becker U and Shirley D 1996 *VUV and Soft X-Ray Photoionization* (New York: Plenum)
[53] Dinu L C, Muller H G, Kazamias S, Mullot G, Augé F, Balcou P, Paul P M, Kovačev M, Breger P and Agostini P 2003 *Phys. Rev. Lett.* **91** 6–9
[54] Aseyev S A, Ni Y, Frasinski L J, Muller H G and Vrakking M J 2003 *Phys. Rev. Lett.* **91** 1–4